Nanomed Res J 11(2):188-198, Spring 2026

RESEARCH ARTICLE

Chloralhydrate Adsorption on the Surface of $C_8B_6N_6$ Nanocluster: A DFT Outlook

Khadijeh Didehban[1], Shoira Ibatova[2], Rustam Turakulov[3], Maxsuda Tuxtayeva[4], Nasiba Nasrulloyeva[5], Akram Hosseinian[6], Sarvin Mohammadi-Aghdam[1], Sepideh Habibzadeh[1*]

[1] Department of Chemistry, Payame Noor University, Tehran, Iran.

[2] Department of Propaedeutics of Children's Diseases, Samarkand State Medical University, Uzbekistan.

[3] Department of Internal Medicine in Family Medicine, Tashkent State Medical University, Tashkent, Uzbekistan.

[4] Department of Hygiene No.2, Bukhara State Medical Institute Abu Ali Ibn Sino, Bukhara, Uzbekistan.

[5] Department of Foreign Languages, University of Economics and Pedagogy, Karshi, Uzbekistan.

[6] Department of Engineering Science, College of Engineering, University of Tehran, Tehran, Iran.

ARTICLE INFO

Article History:
Received: 2026-01-15
Revised: 2026-05-02
Accepted: 2026-05-12

Keywords:
Adsorption
Chloral Hydrate
Density Functional Theory
$C_8B_6N_6$ Nanocluster

ABSTRACT

In this study, the adsorption behavior of chloral hydrate (CH), a toxic sedative and potential environmental contaminant, on a $C_8B_6N_6$ fullerene-like nanocluster was systematically investigated using Density Functional Theory (DFT). Geometry optimizations and frequency calculations were performed at the B3LYP/6-31G* level to explore structural, electronic, and thermodynamic properties in both gaseous and aqueous phases. Three adsorption configurations were analyzed to determine the most stable conformer. The calculated adsorption energies were negative for all configurations, confirming the feasibility of the adsorption process. Among them, the B-conformer exhibited the strongest interaction, with adsorption energies of −102.395 kJ/mol in vacuum and −52.510 kJ/mol in water. The relatively moderate adsorption energies (<150 kJ/mol), absence of bond formation in NBO analysis, and minimal structural distortion indicate that the interaction mechanism is predominantly physisorption. Thermodynamic analyses revealed negative ΔH_ad and ΔG_ad values across the temperature range of 298–318 K, confirming that the adsorption process is exothermic and spontaneous, while lower temperatures favor stronger interactions. Frontier molecular orbital (FMO) analysis demonstrated a significant reduction in the band gap of $C_8B_6N_6$ upon CH adsorption (up to ~52% for the B-conformer), indicating enhanced electronic sensitivity and charge transfer capability. Additionally, adsorption reduced chemical hardness and increased electrophilicity, suggesting improved reactivity and sensing potential. These findings highlight the promising capability of $C_8B_6N_6$ nanoclusters for chloral hydrate adsorption and detection, offering valuable insights for the design of boron nitride-based nanomaterials in environmental remediation and sensor applications.

How to cite this article
Hosseinian A, Ibatova Sh, Turakulov R, Tuxtayeva M, Nasrulloyeva N, Didehban Kh, Mohammadi-Aghdam S, Habibzadeh S. Chloralhydrate Adsorption on the Surface of $C_8B_6N_6$ Nanocluster: A DFT Outlook. Nanomed Res J, 2026; 11(2): 188-198. DOI: 10.22034/nmrj.2026.02.009

INTRODUCTION

Chloral hydrate (CH) is a sedative and hypnotic compound that has been used in medicine for over a century, primarily for its calming and sleep-inducing effects [1]. Chemically, it is a chlorinated derivative of acetaldehyde, and it appears as a colorless crystalline solid that is soluble in water and alcohol [2]. Despite its historical use in treating insomnia and as an anesthetic adjunct, its toxicity and potential for misuse have raised significant concerns [3]. CH can be toxic when consumed in

* Corresponding Author Email: *habibzade@pnu.ac.ir*

This work is licensed under the Creative Commons Attribution 4.0 International License.
To view a copy of this license, visit http://creativecommons.org/licenses/by/4.0/.

excessive amounts, leading to symptoms such as respiratory depression, gastrointestinal distress, cardiac arrhythmias, and even fatal overdose in severe cases [4]. It is metabolized in the body to trichloroethanol, which contributes to its sedative effects but also plays a role in its toxicity [5]. CH can occur as a contaminant or by-product in industrial processes involving chlorinated solvents, making it a potential environmental pollutant [6]. Its presence in water sources or industrial effluents highlights the importance of monitoring and determining its concentration to ensure public safety and environmental protection [7]. Therefore, determination and removal of CH is of great significance. Pharmaceuticals removal from water and wastewater has become a critical environmental concern due to the increasing presence of these contaminants, which can harm aquatic ecosystems and potentially affect human health [8]. Various techniques, such as advanced oxidation processes (AOPs) [9], membrane filtration [10], and biological treatments [11], have been employed to address this issue. However, many of these methods come with significant disadvantages [12]. AOPs, for instance, often require high energy input and the use of expensive chemicals, making them costly and less sustainable in the long term [13]. Membrane filtration, while effective in removing a wide range of contaminants, faces challenges such as membrane fouling, high operating costs, and the generation of concentrated waste streams that require further treatment [14]. Biological treatments, though environmentally friendly, are often limited by the inability of microorganisms to degrade certain pharmaceutical compounds completely, leading to partial treatment and potential formation of harmful by-products [15]. In contrast, adsorption has emerged as a promising alternative for pharmaceutical removal due to its numerous advantages [18]. This technique is highly efficient in capturing a wide range of pharmaceutical compounds, even at low concentrations, through the use of adsorbents such as activated carbon, biochar, or novel nanomaterials [19]. Adsorption processes are relatively simple to operate and do not require complex infrastructure or high energy input, making them cost-effective and sustainable [20]. Additionally, adsorption does not produce harmful by-products or secondary pollution, unlike some chemical methods [21]. The reusability and regeneration of certain adsorbents further enhance the economic and environmental viability of this approach [22]. Overall, adsorption stands out as a practical and efficient solution for addressing pharmaceutical contamination in water systems, overcoming many of the limitations associated with other removal techniques [23]. Pharmaceutical determination techniques play a crucial role in ensuring the safety, efficacy, and quality of drugs [24]. Traditional methods such as spectrophotometry, chromatography, and mass spectrometry have been widely used due to their high sensitivity and ability to provide detailed chemical information [25]. However, these techniques often come with significant disadvantages, including high operational costs, lengthy preparation times, complex sample processing, and the need for highly trained personnel to operate the sophisticated instrumentation [26]. Additionally, many of these methods require the use of hazardous chemicals and solvents, raising environmental and safety concerns [27]. On the other hand, electrochemical sensors have emerged as a promising alternative with several distinct advantages [28]. These sensors are cost-effective, portable, and easy to use, making them particularly suitable for on-site and real-time pharmaceutical analysis [29]. They offer rapid response times and high selectivity while requiring minimal sample preparation [30]. Moreover, electrochemical sensors are more environmentally friendly since they often involve fewer reagents and waste generation [31]. Their ability to be miniaturized and integrated into point-of-care devices further enhances their practicality for widespread applications [32]. As a result, electrochemical sensors are gaining significant attention as a reliable and efficient tool for pharmaceutical determination, addressing many of the limitations posed by traditional methods [33]. However, the first step in the development of a new electrochemical sensor or an adsorptive removal system is finding a material that has a good interaction with the target molecule.

The $C_8B_6N_6$ nanocluster, a fullerene-like structure, exhibits remarkable properties that make it a promising material for adsorption and sensing applications [34]. Its unique composition, consisting of carbon (C), boron (B), and nitrogen (N) atoms, imparts it with a high degree of chemical stability and tunable electronic properties [35]. The presence of boron and nitrogen atoms introduces polar sites within the structure, enhancing its ability to interact with various molecules through dipole-dipole interactions, hydrogen bonding, or van

der Waals forces [36]. This feature is particularly advantageous for adsorption processes, as it allows the nanocluster to effectively capture and hold diverse chemical species [37]. Furthermore, the high surface area of the $C_8B_6N_6$ nanocluster, due to its hollow, cage-like geometry, provides ample active sites for molecular interactions, making it an efficient adsorbent [38]. However, there are certain advantages associated with the $C_8B_6N_6$ nanocluster that also contribute to its functionality as a sensing material [39]. For instance, its electronic structure can be highly sensitive to external perturbations, such as the adsorption of target molecules [40]. Density Functional Theory (DFT) is a powerful and widely used computational quantum mechanical modeling method that has revolutionized the study of electronic structure in materials and molecules [41]. One of its most significant advantages lies in its ability to deliver accurate predictions of the electronic properties of complex systems while remaining computationally efficient compared to other quantum mechanical methods, such as wavefunction-based approaches [42]. This efficiency makes DFT particularly valuable for exploring the adsorption systems of nanostructures, where the interactions between adsorbates and surfaces play a critical role in determining functionality [43]. By employing advanced exchange-correlation functionals, DFT can effectively capture the electronic interactions and binding energies that govern adsorption processes [44]. Furthermore, its flexibility allows researchers to model a wide range of nanostructured materials, including metals, semiconductors, oxides, and 2D materials like graphene or transition metal dichalcogenides [45]. The predictive power of DFT has opened up immense potential for designing and optimizing nanostructures for applications in catalysis, energy storage, sensors, and environmental remediation [46]. For instance, it enables the identification of active sites on catalytic surfaces and provides insights into reaction mechanisms at the atomic level [47]. Additionally, DFT can be combined with machine learning techniques to accelerate the discovery of novel materials with tailored properties [48]. Despite some limitations, such as challenges in accurately describing long-range dispersion interactions or strongly correlated systems, ongoing advancements in computational algorithms and hybrid functionals continue to enhance its accuracy and applicability [49]. Overall, DFT stands as an indispensable tool in modern materials science, offering unparalleled opportunities for understanding and engineering adsorption phenomena in nanostructures [50]. To the best of our knowledge, no prior work has systematically explored the adsorption characteristics of CH on the surface of a $C_8B_6N_6$ nanocluster using DFT methods. This gap in the literature highlights the need for a detailed investigation into the structural and electronic changes that occur during the adsorption process, as well as the thermodynamic feasibility of such interactions. In summary, this study represents a significant step forward in exploring the adsorption behavior of CH on $C_8B_6N_6$ nanoclusters through a DFT-based approach. The findings presented herein will not only enhance our fundamental understanding of molecular-nanocluster interactions but also provide valuable insights for future research and technological applications involving boron nitride-based materials.

Computational Details

In this study, the adsorption of chloral hydrate on the surface of the $C_8B_6N_6$ nanocluster was investigated using Density Functional Theory (DFT) to provide a comprehensive understanding of the interaction mechanisms and associated electronic properties. All computational work was carried out using the Gaussian 16 software package [51], with molecular structure visualization and pre-optimization performed using GaussView 6 [52]. The geometry optimization of the nanocluster and its complexes with chloral hydrate was conducted using the B3LYP [53] hybrid functional, a widely accepted functional for studying molecular systems due to its balanced treatment of exchange and correlation effects. The 6-31G* [54] basis set was employed throughout the study, as it provides a reliable level of accuracy for molecular systems while maintaining computational efficiency. Convergence criteria were carefully monitored to ensure that optimized geometries corresponded to true minima on the potential energy surface, as confirmed by the absence of imaginary frequencies in subsequent frequency calculations. Frequency calculations were performed to evaluate the vibrational modes of the optimized structures and to verify the thermodynamic stability of the adsorption complexes. Infrared (IR) spectra were also simulated to gain insights into potential changes in vibrational characteristics upon adsorption. Thermodynamic parameters,

(cc) BY

including Gibbs free energy (ΔG_{ad}), enthalpy (ΔH_{ad}), thermodynamic equilibrium constant (K_{th}) and entropy (ΔS_{ad}), were calculated to evaluate the feasibility and spontaneity of the adsorption process under standard conditions. To further probe the electronic interactions between chloral hydrate and the $C_8B_6N_6$ nanocluster, frontier molecular orbital (FMO) analysis was conducted. The highest occupied molecular orbital (HOMO) and lowest unoccupied molecular orbital (LUMO) energies were calculated to determine the energy gap (E_g), which provides insights into the electronic stability and reactivity of the system. The density of states (DOS) spectra were analyzed using GaussSum 3 software [55] to visualize the contributions of individual molecular orbitals to the overall electronic structure. Overall, this computational approach allowed for a detailed investigation of the structural, electronic, vibrational, and thermodynamic properties of chloral hydrate adsorption on the $C_8B_6N_6$ nanocluster. The results provide valuable insights into the potential applications of boron nitride-based nanoclusters in adsorption and sensor technologies. To account for environmental effects, single-point energy calculations were conducted using the Polarizable Continuum Model (PCM) [56] with water as the solvent. This approach provides insights into adsorption behavior under realistic conditions. The self-consistent field (SCF) calculations were carried out with a convergence criterion of 10^{-6} Hartree for the total electronic energy. This stringent criterion ensures accurate electronic structure calculations and reliable energy differences between adsorption configurations. To improve convergence, the DIIS (Direct Inversion in the Iterative Subspace) algorithm was used, and initial guesses for molecular orbitals were obtained using the Harris functional. To validate the computational approach, benchmark calculations were carried out by comparing the adsorption energies of a test molecule on a similar nanocluster with available experimental or high-level theoretical data. The results confirmed that the chosen methodology provides reliable predictions within acceptable error margins.

RESULTS AND DISCUSSION

Structural and NBO Analysis

The initial and optimized structures depicted in Fig. 1 clearly illustrate the interaction between the CH molecule and the $C_8B_6N_6$ nanocluster, which has been analyzed in three distinct configurations to identify the most stable conformer. In the

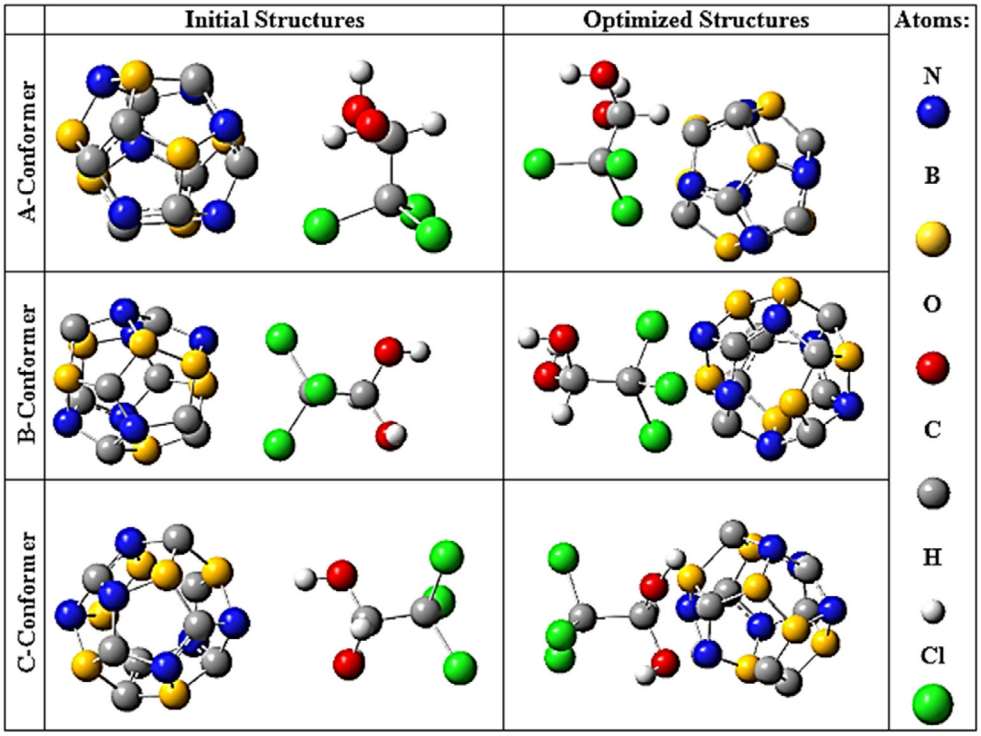


Fig. 1. The initial and optimized structures of CH and $C_8B_6N_6$ complexes

Table 1. Structural properties of CH, $C_8B_6N_6$ and their complexes

Structures	Total electronic energy (a. u.)	Adsorption energy (kJ/mol)	Zero-point energy (kJ/mol)	ν_{min} (cm^{-1})	ν_{max} (cm^{-1})	Dipole moment (Debye)
CH (Vacuum)	-988.771	---	725.516	67.614	4244.939	1.890
CH (Water)	-986.571	---	727.811	67.855	4343.124	2.120
$C_8B_6N_6$ (Vacuum)	-1120.121	---	309.342	398.481	1666.880	0.000
$C_8B_6N_6$ (Water)	-1121.228	---	318.808	399.865	1663.231	0.020
A-Conformer (Vacuum)	-2108.912	-52.510	1121.955	43.820	3793.852	5.969
A-Conformer (Water)	-2107.807	-21.004	1126.655	45.539	3794.492	6.599
B-Conformer (Vacuum)	-2108.931	-102.395	1138.622	36.958	4247.733	7.609
B-Conformer (Water)	-2107.819	-52.510	1123.309	37.797	4249.980	8.579
C-Conformer (Vacuum)	-2108.923	-81.391	1127.809	37.181	4332.898	9.499
C-Conformer (Water)	-2107.812	-34.132	1132.111	39.650	4334.968	10.469

A-Conformer, the CH molecule is oriented parallel to the nanocluster, positioned adjacent to its side chlorine and hydrogen atoms. In the B-Conformer, the CH molecule is situated near the $C_8B_6N_6$ nanocluster, with its chlorine atoms directed towards the cluster. Lastly, in the C-Conformer, the CH molecule is positioned close to the nanocage, oriented towards its OH groups. As illustrated in Fig. 1, both the initial and optimized structures demonstrate that no significant structural distortions have occurred during the geometrical optimization process [57]. Therefore, the interactions appear to be relatively weak, suggesting that a physisorption mechanism predominates across all configurations [58]. The results obtained are summarized in Table 1. As observed, the total electronic energy of the B-Conformer is more negative compared to the A and C configurations [59]. This indicates that the interactions within the B-Conformer are stronger, making its formation more experimentally favorable. The calculated adsorption energies are summarized in Table 1. As evident, all the obtained adsorption energies for the three different conformers are negative, indicating that the adsorption process is experimentally feasible [60]. Among them, the adsorption energy of the B-Conformer is lower compared to those of the A and C configurations, suggesting that the formation of the B-Conformer is energetically more favorable than the others [61]. The effect of water as a solvent was also examined using the PCM solvation method. The results, presented in Table 1, reveal that while the adsorption energy values slightly decrease in the aqueous phase, they remain negative [62]. This observation suggests that the adsorption process is still experimentally feasible in the aqueous phase, although the interactions are somewhat weaker compared to those in the gaseous phase [63].

The adsorption energy values for all examined conformers, in both gaseous and aqueous phases, are below 150 kJ/mol, suggesting that the adsorption mechanism is likely physisorption [64]. To gain deeper insights into the adsorption mechanism, natural bond orbital (NBO) calculations were performed on the optimized structures [65]. The results confirmed the absence of any bond formation between the adsorbate and the adsorbent, further validating that the adsorption mechanism is definitively physisorption [66]. Following the geometrical optimization, IR calculations were performed on all evaluated structures. The maximum and minimum calculated IR frequencies are presented in Table 1. As observed, no negative values were obtained, indicating that all the analyzed structures represent true local minima [67].

Thermodynamic Parameters

The thermodynamic parameters calculated for the study are summarized in Table 2. The data clearly indicate that the adsorption process is highly exothermic and spontaneous. This conclusion is supported by the consistently negative values of both ΔH_{ad} and ΔG_{ad} across all three conformers, regardless of whether the process occurs in the aqueous or gaseous phase. These negative values signify that the adsorption releases energy (exothermic nature) and proceeds without the need for external input (spontaneity) [68]. The values of K_{th} suggest that the interactions are reversible and exist in a state of equilibrium, indicating a dynamic balance between adsorption and desorption processes [69]. The negative values of ΔS_{ad} imply that the interactions are not favorable from an entropy perspective, likely due

(cc) BY

Table 2. The calculated thermodynamic parameters in 298-318 K at 10° intervals

NO	ΔH_{ad} (kJ/mol)	ΔG_{ad} (kJ/mol)	ΔS_{ad} (J/mol)	K_{th}
A-Conformer-Vacuum-298	-63.381	-65.812	-141.891	$3.392\times10^{+11}$
A-Conformer-Vacuum-308	-61.040	-63.471	-144.450	$5.746\times10^{+10}$
A-Conformer-Vacuum-318	-58.699	-61.130	-147.012	$1.089\times10^{+10}$
A-Conformer-Water-298	-31.875	-34.306	-136.103	$1.024\times10^{+06}$
A-Conformer-Water-308	-29.534	-31.965	-138.665	$2.622\times10^{+05}$
A-Conformer-Water-318	-27.193	-29.624	-142.221	$7.310\times10^{+04}$
B-Conformer-Vacuum-298	-113.266	-115.697	-123.699	$1.864\times10^{+20}$
B-Conformer-Vacuum-308	-110.925	-113.356	-126.260	$1.643\times10^{+19}$
B-Conformer-Vacuum-318	-108.584	-111.015	-128.828	$1.688\times10^{+18}$
B-Conformer-Water-298	-63.381	-65.812	-134.212	$3.392\times10^{+11}$
B-Conformer-Water-308	-61.040	-63.471	-132.069	$5.746\times10^{+10}$
B-Conformer-Water-318	-58.699	-61.130	-134.638	$1.089\times10^{+10}$
C-Conformer-Vacuum-298	-92.262	-94.693	-136.743	$3.894\times10^{+16}$
C-Conformer-Vacuum-308	-89.921	-92.352	-139.302	$4.521\times10^{+15}$
C-Conformer-Vacuum-318	-87.580	-90.011	-141.868	$6.008\times10^{+14}$
C-Conformer-Water-298	-45.003	-47.434	-129.889	$2.044\times10^{+08}$
C-Conformer-Water-308	-42.662	-45.093	-132.456	$4.406\times10^{+07}$
C-Conformer-Water-318	-40.321	-42.752	-135.015	$1.046\times10^{+07}$

to the aggregation of nanoclusters following the adsorption process [70]. This aggregation reduces the system's disorder, thereby contributing to the unfavorable entropy change. The influence of temperature on all thermodynamic parameters was thoroughly examined. The findings reveal that as the temperature increases, both ΔH_{ad} (enthalpy change) and ΔG_{ad} (Gibbs free energy change) become more positive [71]. This suggests that the adsorption process becomes less thermodynamically favorable with rising temperature. On the other hand, the values of ΔSad (entropy change) and K_{th} (equilibrium constant) decrease as temperature increases, further indicating that the interactions are more energetically and entropically favorable at lower temperatures [72]. This behavior highlights that lower temperatures promote stronger and more stable interactions, while higher temperatures disrupt the equilibrium, making the adsorption process less efficient [73].

FMO Analysis

The examination of frontier molecular orbital (FMO) parameters, as detailed in Table 3 and Fig. 3, reveals significant changes in the band gap of $C_8B_6N_6$ upon adsorption. Initially measured at 2.178 eV, the band gap decreases markedly to 1.392 eV, 1.046 eV, and 1.315 eV for conformers A, B, and C, respectively. This represents a substantial maximum reduction of approximately 51.997% for the most favorable conformer. Such a dramatic decline in the band gap highlights the remarkable potential of $C_8B_6N_6$ as an effective electrocatalyst modifier, particularly for detecting CH molecules [74]. The decrease in the band gap indicates an enhanced electronic interaction between $C_8B_6N_6$ and the adsorbed species, which could lead to improved charge transfer properties [75]. This is a crucial characteristic for materials used in electrocatalysis, as it directly impacts their sensitivity and efficiency in detecting specific molecules [76]. The variation in band gap values across different conformers suggests that the structural configuration of $C_8B_6N_6$ plays a pivotal role in its electronic properties and interaction with adsorbates. The results underscore the adaptability of $C_8B_6N_6$ as a tunable material, with conformer B showing the most significant reduction in band gap [77]. This makes it particularly promising for applications requiring precise and efficient molecular detection. The findings pave the way for further exploration of $C_8B_6N_6$ in advanced sensor technologies and electrocatalytic systems, where its ability to modify electronic properties upon interaction with target molecules could be harnessed for innovative solutions in chemical sensing and energy applications [78]. The adsorption process leads to a noticeable decrease in the chemical hardness of CH, reducing it from its initial value of 3.472 eV to 0.696 eV, 0.523 eV, and 0.657 eV for the respective conformers. This reduction in chemical hardness signifies an

CC BY

Table 3. The computed FMO parameters

Structures	E_{HOMO} (eV)	E_{LUMO} (eV)	Eg (eV)	%ΔEg	η (eV)	μ (eV)	ω (eV)	ΔN_{max} (eV)
CH	-8.390	-1.446	6.944	---	3.472	-4.918	3.484	1.417
$C_8B_6N_6$	-5.750	-3.572	2.178	---	1.089	-4.661	9.973	4.280
A-Conformer	-4.830	-3.438	1.392	-36.098	0.696	-4.134	12.279	5.940
B-Conformer	-4.155	-3.109	1.046	-51.977	0.523	-3.632	12.614	6.945
C-Conformer	-4.788	-3.473	1.315	-39.631	0.657	-4.130	12.973	6.282

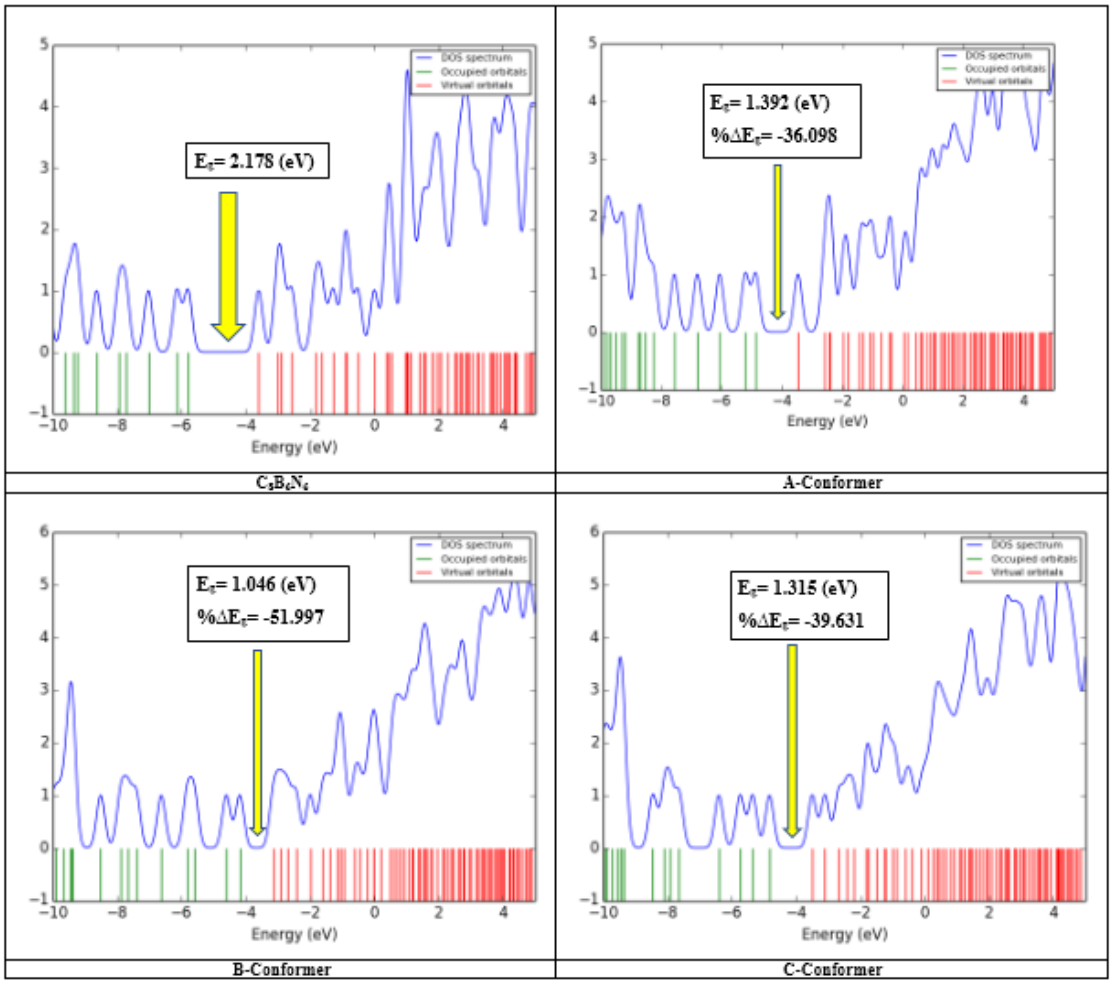


Fig. 2. The computed DOS spectrums

increase in chemical reactivity after adsorption, as lower chemical hardness typically correlates with a greater tendency to participate in chemical reactions [79]. Moreover, the negative values of chemical potential observed in these configurations provide further evidence of their thermodynamic stability. These findings indicate that the adsorption process not only enhances the chemical reactivity of CH but also significantly stabilizes the resulting conformers [80]. This stabilization makes these conformers more favorable for practical applications in a wide range of chemical and material systems [81-83]. Furthermore, the process of adsorption leads to notable increases in both the electrophilicity index and the maximum charge transfer capacity for CH when adsorbed onto the $C_8B_6N_6$ surface. This suggests that the interaction with the nanostructured surface substantially boosts CH's ability to absorb electrons, a capability that is markedly reduced in isolated CH molecules without such interactions [84]. These insights highlight the transformative role of adsorption in

improving the electronic properties and functional potential of CH, opening up new avenues for its use in advanced material design, catalysis, and other technological applications.

CONCLUSION

In this work, the adsorption behavior of chloral hydrate (CH) on a $C_8B_6N_6$ fullerene-like nanocluster was comprehensively investigated using Density Functional Theory calculations. Three different adsorption configurations were examined in both gaseous and aqueous phases to determine the most stable interaction mode. The calculated adsorption energies were negative for all conformers, confirming the thermodynamic feasibility of the adsorption process. Among the studied configurations, the B-conformer exhibited the strongest interaction and highest stability, making it the most favorable adsorption structure. The magnitude of adsorption energies (below 150 kJ/mol), absence of new bond formation from NBO analysis, and negligible structural distortions collectively indicate that the adsorption mechanism is predominantly physisorption. Solvent effects slightly weakened the interactions but did not alter the spontaneous nature of the process. Thermodynamic parameters further confirmed that the adsorption is exothermic and spontaneous across the investigated temperature range (298–318 K), with lower temperatures favoring stronger adsorption. The negative entropy changes suggest increased order upon adsorption, consistent with adsorbate–adsorbent association. Frontier molecular orbital analysis revealed a significant reduction in the band gap of $C_8B_6N_6$ after CH adsorption, particularly for the B-conformer, indicating enhanced electronic sensitivity and charge transfer characteristics. The decrease in chemical hardness and increase in electrophilicity and maximum charge transfer capacity further demonstrate that adsorption substantially modifies the electronic properties of the nanocluster. These electronic changes highlight the strong potential of $C_8B_6N_6$ as a sensing material for chloral hydrate detection. Overall, this theoretical study provides valuable molecular-level insight into the interaction mechanism between CH and $C_8B_6N_6$ nanoclusters. The results suggest that $C_8B_6N_6$ is a promising candidate for chloral hydrate adsorption and sensor development, particularly in environmental monitoring applications. Future experimental validation and exploration of functionalized derivatives may further enhance their practical applicability.

CONFLICT OF INTEREST STATEMENT

The authors declare that there are no conflicts of interest related to the research, authorship, or publication of this manuscript. All authors have disclosed any financial or personal relationships that could potentially influence or bias the work presented.

REFERENCES

1. Bruzzoniti MC, Mentasti E, Sarzanini C, Tarasco E. Liquid chromatographic methods for chloral hydrate determination. J Chromatogr A. 2001;920(1-2):283-289. https://doi.org/10.1016/S0021-9673(01)00554-4
2. Dąbrowska A, Nawrocki J. Controversies about the occurrence of chloral hydrate in drinking water. Water Res. 2009;43(8):2201-2208. https://doi.org/10.1016/j.watres.2009.02.022
3. Schmitt TC. Determination of chloral hydrate and its metabolites in blood plasma by capillary gas chromatography with electron capture detection. J Chromatogr B Analyt Technol Biomed Life Sci. 2002;780(2):217-224. https://doi.org/10.1016/S1570-0232(02)00371-9
4. Browne JC. Chloral hydrate: its inconveniences and dangers. Lancet. 1871;97(2484):473-475. https://doi.org/10.1016/S0140-6736(02)69339-0
5. Meyer E, Van Bocxlaer JF, Lambert WE, Piette M, De Leenheer AP. Determination of chloral hydrate and metabolites in a fatal intoxication. J Anal Toxicol. 1995;19(2):124-126. https://doi.org/10.1093/jat/19.2.124
6. Barrott L. Chloral hydrate: formation and removal by drinking water treatment. J Water Supply Res Technol AQUA. 2004;53(6):381-390. https://doi.org/10.2166/aqua.2004.0030
7. Dąbrowska A, Nawrocki J. Controversies about the occurrence of chloral hydrate in drinking water. Water Res. 2009;43(8):2201-2208. https://doi.org/10.1016/j.watres.2009.02.022
8. Rivera-Utrilla J, Sánchez-Polo M, Ferro-García MÁ, Prados-Goya J, Ocampo-Pérez R. Pharmaceuticals as emerging contaminants and their removal from water. A review. Chemosphere. 2013;93(7):1268-1287. https://doi.org/10.1016/j.chemosphere.2013.07.059
9. Mansouri F, Chouchene K, Roche N, Ksibi M. Removal of pharmaceuticals from water by adsorption and advanced oxidation processes: state of the art and trends. Appl Sci (Basel). 2021;11(14):6659. https://doi.org/10.3390/app11146659
10. Alfonso-Muniozguren P, Serna-Galvis EA, Bussemaker M, Torres-Palma RA, Lee J. A review on pharmaceuticals removal from waters by single and combined biological, membrane filtration and ultrasound systems. Ultrason Sonochem. 2021;76:105656. https://doi.org/10.1016/j.ultsonch.2021.105656
11. Tiwari B, Sellamuthu B, Ouarda Y, Drogui P, Tyagi RD, Buelna G. Review on fate and mechanism of removal of pharmaceutical pollutants from wastewater using

CC BY

biological approach. Bioresour Technol. 2017;224:1-12. https://doi.org/10.1016/j.biortech.2016.11.042
12. Calisto V, Ferreira CI, Oliveira JA, Otero M, Esteves VI. Adsorptive removal of pharmaceuticals from water by commercial and waste-based carbons. J Environ Manage. 2015;152:83-90. https://doi.org/10.1016/j.jenvman.2015.01.019
13. Akhtar J, Amin NAS, Shahzad K. A review on removal of pharmaceuticals from water by adsorption. Desalin Water Treat. 2016;57(27):12842-12860. https://doi.org/10.1080/19443994.2015.1051121
14. Bui TX, Choi H. Adsorptive removal of selected pharmaceuticals by mesoporous silica SBA-15. J Hazard Mater. 2009;168(2-3):602-608. https://doi.org/10.1016/j.jhazmat.2009.02.072
15. Huang L, Shen R, Shuai Q. Adsorptive removal of pharmaceuticals from water using metal-organic frameworks: A review. J Environ Manage. 2021;277:111389. https://doi.org/10.1016/j.jenvman.2020.111389
16. Kyzas GZ, Fu J, Lazaridis NK, Bikiaris DN, Matis KA. New approaches on the removal of pharmaceuticals from wastewaters with adsorbent materials. J Mol Liq. 2015;209:87-93. https://doi.org/10.1016/j.molliq.2015.05.025
17. Thakur A, Kumar A, Singh A. Adsorptive removal of heavy metals, dyes, and pharmaceuticals: Carbon-based nanomaterials in focus. Carbon. 2024;217:118621. https://doi.org/10.1016/j.carbon.2023.118621
18. Seo PW, Bhadra BN, Ahmed I, Khan NA, Jhung SH. Adsorptive removal of pharmaceuticals and personal care products from water with functionalized metal-organic frameworks: remarkable adsorbents with hydrogen-bonding abilities. Sci Rep. 2016;6:34462. https://doi.org/10.1038/srep34462
19. Sekulic MT, Boskovic N, Slavkovic A, Garunovic J, Kolakovic S, Pap S. Surface functionalised adsorbent for emerging pharmaceutical removal: adsorption performance and mechanisms. Process Saf Environ Prot. 2019;125:50-63. https://doi.org/10.1016/j.psep.2019.03.007
20. Wang T, He J, Lu J, Zhou Y, Wang Z, Zhou Y. Adsorptive removal of PPCPs from aqueous solution using carbon-based composites: A review. Chin Chem Lett. 2022;33(8):3585-3593. https://doi.org/10.1016/j.cclet.2021.09.029
21. Aljeboree AM, Alshirifi AN. Adsorption of Pharmaceuticals as emerging contaminants from aqueous solutions on to friendly surfaces such as activated carbon: A review. J Pharm Sci Res. 2018;10(9):2252-2257.
22. An HJ, Bhadra BN, Khan NA, Jhung SH. Adsorptive removal of wide range of pharmaceutical and personal care products from water by using metal azolate framework-6-derived porous carbon. Chem Eng J. 2018;343:447-454. https://doi.org/10.1016/j.cej.2018.03.025
23. Vona A, Di Martino F, Garcia-Ivars J, Picó Y, Mendoza-Roca JA, Iborra-Clar MI. Comparison of different removal techniques for selected pharmaceuticals. J Water Process Eng. 2015;5:48-57. https://doi.org/10.1016/j.jwpe.2014.12.011
24. Ternes TA. Analytical methods for the determination of pharmaceuticals in aqueous environmental samples. TrAC Trends Anal Chem. 2001;20(8):419-434. https://doi.org/10.1016/S0165-9936(01)00078-4
25. Gilpin RK, Gilpin CS. Pharmaceuticals and related drugs. Anal Chem. 2007;79(12):4275-4294. https://doi.org/10.1021/ac070708x
26. Gilpin RK, Gilpin CS. Pharmaceuticals and related drugs. Anal Chem. 2009;81(12):4679-4694. https://doi.org/10.1021/ac900804d
27. Cini N, Gölcü A. Spectrophotometric methodologies applied for determination of pharmaceuticals. Curr Anal Chem. 2021;17(8):1141-1168. https://doi.org/10.2174/1573411016999200526133357
28. Uslu B, Ozkan SA. Electroanalytical methods for the determination of pharmaceuticals: a review of recent trends and developments. Anal Lett. 2011;44(16):2644-2702. https://doi.org/10.1080/00032719.2011.553010
29. Dubenska L, Blazhejevskyj M, Plotycya S, Pylypets MY, Sarahman OM. Voltammetric methods for the determination of pharmaceuticals. Methods Objects Chem Anal. 2017;12(2):61-75. https://doi.org/10.17721/moca.2017.61-75
30. Feier B, Florea A, Cristea C, Săndulescu R. Electrochemical detection and removal of pharmaceuticals in waste waters. Curr Opin Electrochem. 2018;11:1-11. https://doi.org/10.1016/j.coelec.2018.06.012
31. Bitew Z, Amare M. Recent reports on electrochemical determination of selected antibiotics in pharmaceutical formulations: A mini review. Electrochem Commun. 2020;121:106863. https://doi.org/10.1016/j.elecom.2020.106863
32. Boumya W, Taoufik N, Achak M, Bessbousse H, Elhalil A, Barka N. Electrochemical sensors and biosensors for the determination of diclofenac in pharmaceutical, biological and water samples. Talanta Open. 2021;3:100026. https://doi.org/10.1016/j.talo.2020.100026
33. Lenik J. Cyclodextrins based electrochemical sensors for biomedical and pharmaceutical analysis. Curr Med Chem. 2017;24(22):2359-2391. https://doi.org/10.2174/0929867323666161213101407
34. Niknam Rad P, Qomi M, Jalali Sarvestani MR. DFT Studies on the Sulfamethoxazole Interactions with C8B6N6 Nanocluster. Nanomed Res J. 2024;9(2):206-212.
35. Razeghi MH, Gholipour O, Arabi S, Nemati-Kande E, Jahanbin Sardroodi J. A DFT Outlook on Bupropion Adsorption on the Surface of C8B6N6 Nanocluster. Int J New Chem. 2025;12(4):903-921.
36. Behnia A, Jalali Sarvestani MR, Abdulmutaleb Ibrahim A, Mahdi MS. DFT studies on the nalidixic acid interactions with C8B6N6 nanocluster. Chem Rev Lett. 2024;7(6):993-1000.
37. Yousefi M, Rad MS, Shakibazadeh R, Ghodrati L, Kachoie MA. Simulating a heteroatomic CBN fullerene-like nanocage towards the drug delivery of fluorouracil. Mol Simul. 2022;48(14):1284-1292. https://doi.org/10.1080/08927022.2022.2086252
38. Ahmadi R. Furazolidone Adsorption on the Surface of B12N12: DFT Simulations. J Med Med Chem. 2025;1(3):100-105.
39. Mirderikvand N, Mahboubi-Rabbani M. A DFT Study on Citalopram Adsorption on the Surface of B12N12. J Chem Technol. 2025;1(3):90-95.
40. Noqani H, Behnia A. Clomipramine Interaction with B12N12: DFT Simulations. J Med Med Chem. 2025;1(4):118-123.
41. Orio M, Pantazis DA, Neese F. Density functional theory.

(cc) BY

Photosynth Res. 2009;102(2-3):443-453. https://doi.org/10.1007/s11120-009-9404-8
42. Bartolotti LJ, Flurchick K. An introduction to density functional theory. Rev Comput Chem. 1996;9:187-216. https://doi.org/10.1002/9780470125847.ch4
43. Engel E. Density Functional Theory. Berlin: Springer-Verlag; 2011. https://doi.org/10.1007/978-3-642-14090-7
44. Geerlings P, De Proft F, Langenaeker W. Conceptual density functional theory. Chem Rev. 2003;103(5):1793-1874. https://doi.org/10.1021/cr990029p
45. Gross EK, Dreizler RM, editors. Density Functional Theory. New York: Springer Science & Business Media; 2013.
46. Argaman N, Makov G. Density functional theory: An introduction. Am J Phys. 2000;68(1):69-79. https://doi.org/10.1119/1.19375
47. Burke K. Perspective on density functional theory. J Chem Phys. 2012;136(15):150901. https://doi.org/10.1063/1.4704546
48. Cohen AJ, Mori-Sánchez P, Yang W. Challenges for density functional theory. Chem Rev. 2012;112(1):289-320. https://doi.org/10.1021/cr200107z
49. Harrison NM. An introduction to density functional theory. NATO Sci Ser III Comp Syst Sci. 2003;187:45-70.
50. Kohn W, Becke AD, Parr RG. Density functional theory of electronic structure. J Phys Chem. 1996;100(31):12974-12980. https://doi.org/10.1021/jp960669l
51. Frisch MJ, Trucks GW, Schlegel HB, Scuseria GE, Robb MA, Cheeseman JR, et al. Gaussian 16, Revision C.01. Wallingford CT: Gaussian, Inc.; 2016.
52. Dennington R, Keith TA, Millam JM. GaussView, Version 6. Shawnee Mission KS: Semichem Inc.; 2016.
53. Tirado-Rives J, Jorgensen WL. Performance of B3LYP density functional methods for a large set of organic molecules. J Chem Theory Comput. 2008;4(2):297-306. https://doi.org/10.1021/ct700248k
54. Rassolov VA, Ratner MA, Pople JA, Redfern PC, Curtiss LA. 6-31G* basis set for third-row atoms. J Comput Chem. 2001;22(9):976-984. https://doi.org/10.1002/jcc.1058
55. O'Boyle NM, Tenderholt AL, Langner KM. cclib: A library for package-independent computational chemistry algorithms. J Comput Chem. 2008;29(5):839-845. https://doi.org/10.1002/jcc.20823
56. Mennucci B. Polarizable continuum model. Wiley Interdiscip Rev Comput Mol Sci. 2012;2(3):386-404. https://doi.org/10.1002/wcms.1086
57. Alirezapour F, Bamdad K, Jokar M, Khanmohammadi A. A computational insight into structural analysis and electronic properties of altretamine anticancer drug complexed with group IIA (Mg2+, Ca2+) metal ions, quasi-metal (Si2+, Ge2+) ions, and transition metal (Fe2+, Zn2+) ions. Chem Rev Lett. 2026;9(1):209-222.
58. Narkulov O, Soxibova UN, Qalandarov U, Urunova X, Haydarova G, Boliyeva LS, et al. DFT studies on HCN gas detection by pristine and Li decorated Triazasumanene nanostructures. Chem Rev Lett. 2026;9(1):230-242.
59. Abdellah E, Omar B. DFT calculations of structural, elastic, electronic and optical properties of CaXH3 (X= Co, Rh). Chem Rev Lett. 2026;9(1):169-178.
60. Haqgu M, Rostami Z, Mengboev A. DFT investigation of aflatoxin B1 adsorption on vacancy-defective graphene: electronic properties and sensing potential. Chem Rev Lett. 2025;8(6):1258-1268.
61. Behjatmanesh-Ardakani R, Mohammadi-Manesh H, Sedaghatjo M. Pt-embedded pyrrolic and pyridinic N-doped graphene quantum dots as a viable aflatoxin B1 sensor: Insights from DFT calculations. Chem Rev Lett. 2025;8(5):1003-1017.
62. Hamad AA, Kaka KN, Omer RA. Cyclopentanone-based chalcone derivatives: Synthesis, characterization, DFT, drug-likeness and molecular docking studies. Chem Rev Lett. 2025;8(5):1036-1060.
63. Saadh MJ, Hsu CY, Kareem RA, Jafarova AM, Zareii A, Edalat M, et al. Computational assessments of 5-Fluorocytosine (Flucytosine) antifungal adsorption onto a fullerene oxide nanocage for engineering a potential drug delivery platform. Chem Rev Lett. 2025;8(3):547-554.
64. Vaziri I, Amini I, Poor Heravi MR, Rzayev R. A density functional theory study of adsorption dimethyl fumarate on the surface of the pristine of g-C3N4 and Fe, Ni and Cu decorated graphitic carbon nitride. Chem Rev Lett. 2025;8(1):52-67.
65. Behjatmanesh-Ardakani R, Rzayev R. Hydrogen assisted SO2 dissociation on the Pt-doped graphene quantum dot surface: a non-periodic DFT study. Chem Rev Lett. 2025;8(1):178-186.
66. Behjatmanesh-Ardakani R, Magkoev TT. SO2 adsorption and its direct proportional dissociation on the Cu (100), Cu (110), and Cu (111) surfaces: a periodic DFT study. Chem Rev Lett. 2024;7(5):873-883.
67. Ghnim ZS, Adthah AH, Mahdi MS, Mansoor AS, Radi UK, Abd NS, et al. Enhanced adsorption performance and efficiency of graphitic GaN monolayers through functionalizing with transition metal adatoms (Co, Cu and Ni): A DFT study. Chem Rev Lett. 2024;7(6):912-925.
68. Mahdi MS, Mushtaq H, Hasan DF, Bahir H, Idan AH, Behmagham F. Electronic and optical properties of 2D VFeSb: case study by DFT. Chem Rev Lett. 2024;7(6):964-971.
69. Behjatmanesh-Ardakani R, Rzayev R. Pd-and Pt-doped graphene quantum dots for SO2 adsorption and dissociation: A non-periodic DFT study. Chem Rev Lett. 2024;7(6):1022-1030.
70. Jameel RK, Hamid Abbas Al-Anbari H, Salah Mansoor A, Hasan Kadhem A, Bahair H, Abbasi V. Characterization of tetramethyl guanidinium 4-nitro phenoxide (TMG-NP) and tetraphenyl guanidinium 4-nitro phenoxide (TPG-NP) as new ionic liquids (ILs) using DFT and ab initio. Chem Rev Lett. 2024;7(4):661-676.
71. Al-Sattar Dawood AA, Abdul Hussein AH, Al-Shami KR, Azizi B, Thabit R, MH H, et al. Electronic and magnetic structure of monolayer MnAs (111): a case study by DFT. Chem Rev Lett. 2024;7(3):373-379.
72. Hoseyni SJ, Karbakhshzadeh A, Moshtaghi Zonouz A, Husseen B. Computational investigation on interaction between graphene nanostructure BC3 and antiparkinson drug amantadine: Possible sensing study of BC3 and its doped derivatives on amantadine. Chem Rev Lett. 2024;7(3):380-387.
73. Alimohammadi F, Rezanejade Bardajee G, Monfared A. The sensing behavior of MgO nanotube to thiopropamine drug via DFT investigation. Chem Rev Lett. 2024;7(3):513-521.
74. Kamalinahad S, Saud HR, Bashir H, Qassem TA, Tariq H. Theoretical Study on the Enhancement of Nonlinear

CC BY

Optical and Electronic Responses of Sumanene through Interaction with Alkali Metals (Li, Na, and K). Chem Rev Lett. 2024;7(2):173-184.
75. Ahmadi S, Habibzadeh S, Didehban K, Kheirollahi Nezhad PD, Mohammadi R, Rostami Z. Acrylamide Adsorption on the Surfaces of Pristine, B, N and Si-doped Fullerenes: A Comparative DFT Study. Chem Res Technol. 2026;3(2):68-77.
76. Mohasseb A. Carbamazepine Adsorption on the Surface of Carbon Nanocone: DFT Studies. Comp Chem Biol. 2026;1(1):14-21.
77. Tavassoli A. Computational Exploration of Gefitinib-BC3 Interactions: Influence of Al, Ga and Si Doping on Adsorption and Coordination Modes. Comp Chem Biol. 2026;1(1):31-46.
78. Badrzadeh D, Ahmadi R, Sheshmani S, Khalil Moghadam S, Shahvelayati AS. Gingerol interaction with BN nanocone: a comprehensive theoretical study. Chem Sci Res. 2026;1(1):7-12.
79. Ahmadi R. Curcumin Adsorption on the Surface of Al12P12 Nanocluster: DFT Simulations. Comp Chem Biol. 2026;1(1):55-60.
80. Arabi S. Applications of Artificial Intelligence to Computational Chemistry. Comp Chem Biol. 2026;1(2):61-71.
81. Baeelashaki R. Computational Approaches in Veterinary Drug Discovery: From Molecular Docking to Artificial Intelligence. Comp Chem Biol. 2026;1(2):72-86.
82. Zarei K, Amini A, Kafi Moghaddam A, Mahboubi-Rabbani M, Bayanati M. Computational Chemistry in Drug Discovery: A Review of Methodologies and Applications from Target Identification to Drug Optimization. Comp Chem Biol. 2026;1(2):87-96.
83. Chima Ubah P, Donatus RB, Uken AD, Adam AB, Ataitiya H, Abubakar M, et al. Computational Modeling and Density Functional Theory (DFT) Insights into the Structure-Activity Relationship of Bioactive Organic Compounds in Drug Discovery. Comp Chem Biol. 2026;1(2):110-123.
84. Shuheil MA, Zalov AZ, Imanov HA, Huseynova AT, Majeed Alrufaie MM, Jalali Sarvestani MR. Electrochemical determination of Ag+ in industrial effluents by coated graphite potentiometric sensor based on phenothiazine-based ligand as the ionophore: DFT and experimental studies. Int J Environ Anal Chem. 2026:1-7. https://doi.org/10.1080/03067319.2026.2666865